Materials Theory and Modelling

EDITORS

Jeremy Broughton
Paul Bristowe
John Newsam

MRS

COMPUTATIONAL DIAGNOSTICS FOR DETECTING PHASE TRANSITIONS DURING NANOINDENTATION

Susanne M. Lee*, Carol G. Hoover*, Jeffrey S. Kallman*, William G. Hoover*[†],
Anthony J. De Groot*, and Frederick Wooten[†]

* Lawrence Livermore National Laboratory, P. O. Box 808, Livermore, California 94551.

[†] Department of Applied Science, UC Davis/Livermore, Livermore, California 94551.

ABSTRACT

We study nanoindentation of silicon using nonequilibrium molecular dynamics simulations with up to a million particles. Both crystalline and amorphous silicon samples are considered. We use computational diffraction patterns as a diagnostic tool for detecting phase transitions resulting from structural changes. Simulations of crystalline samples show a transition to the amorphous phase in a region a few atomic layers thick surrounding the lateral faces of the indentor, as has been suggested by experimental results. Our simulation results provide estimates for the yield strength (nanohardness) of silicon for a range of temperatures.

INTRODUCTION

Nanometer-machining techniques, using the diamond turning machine at Livermore, produce highly-polished surfaces which are flat to an accuracy of three atomic layers. The production rate is approximately one square meter per year. This slow rate, however, is not economically feasible for large production runs. The surface quality of the samples produced can be measured with scanning tunneling and atomic force microscopy. Sub-surface damage, such as internal cracks, is not measurable. Our work aims to develop parameter guidelines for nanometer-machining experiments and to study surface and bulk characteristics of ceramics and metals.

Experiments show that brittle materials, such as silicon and glass, will flow plastically, rather than crack and fracture, for sufficiently small specimen sizes. Nanoindentation, the simplest experiment for measuring material hardness, is a valuable tool for quantifying ductile and brittle behavior and transitions between solid phases of silicon. The experimental samples are a micron in size and the indentation tool tip diameter is typically about 30 nanometers. In this work we simulate the nanoindentation of amorphous and crystalline silicon with nonequilibrium molecular dynamics. We study phase transitions with computer-simulated x-ray diffraction patterns to detect structural modifications. The simulated diffraction patterns augment the visualization of the sample in real space. Measured yield strengths provide a quantitative comparison with experiments.

The speed and storage capacity of massively-parallel computers make possible atomistic simulations of tens of millions of particles in three dimensions. This provides the opportunity to study the ductile or brittle behavior as a function of the size of the silicon sample. The results reported here are for sample sizes up to a million particles.

COMPUTATION

Nonequilibrium molecular dynamics simulates systems which exchange both heat and work with their surroundings. We perform the indentation under isothermal conditions with the crystal kept at an average temperature, T, and average kinetic energy, $<K>=3kT/2$ per

atom. Details of the simulation technique are given in the references[1,2,3]. The Nosé-Hoover equations of motion are given by

$$\dot{p} = -\nabla\Phi - \zeta p \; ; \; \dot{\zeta} = [(K /< K_O >) - 1]/\tau^2 .$$

Here ζ is an integral-feedback friction coefficient and τ is the energy relaxation time for the feedback mechanism. The friction coefficient takes on both positive values (heat loss) and negative values (heat gain) to maintain the crystal at the specified average temperature. The silicon atoms interact with a Stillinger-Weber potential[4]. We have selected this potential to model the covalent bonding (three body forces) in silicon. For comparison with experiments we model a tetrahedral-shaped indentation tool either as a rough surface, with atoms in a diamond cubic lattice, or as a smooth surface. An indentation simulation is shown in Figure 1. The silicon interactions with the perfectly smooth indentor are normal to the surface and are modeled by an image atom on the inside of the indentor. In both the smooth and atomistic indentor cases, the interactions with silicon are modeled with the repulsive part of a Lennard-Jones potential.
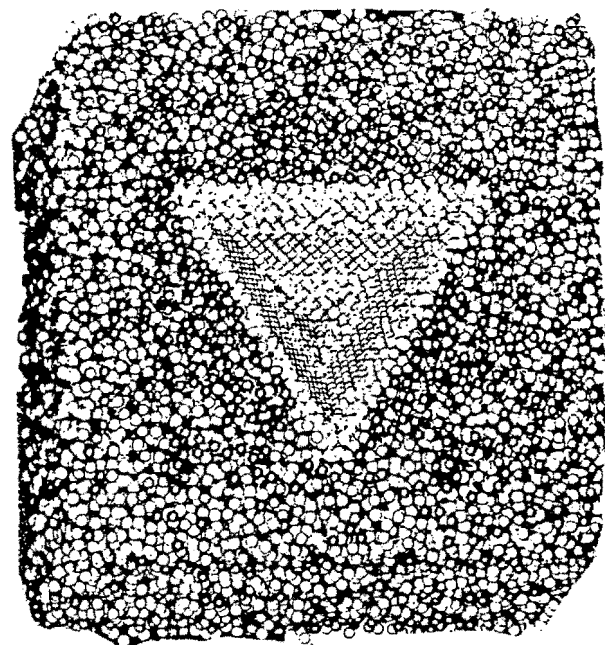
Figure 1. Top view of the indentation geometry for 32,768 particles. This is at the end of the deformation with the indentor removed.

We have developed complementary computer diagnostic techniques (color-coded atoms displayed in real space and reciprocal-space diffraction patterns) for analyzing the results of the molecular dynamics simulations. We visualize results in real space in two ways. First, we color code the atoms based on their current position. This is useful in viewing the volume of the crystal carved out by the indentor as illustrated in the top view shown in Figure 1. Alternatively, we use a color coding based on the initial position of the atom. Both methods are valuable for qualitatively analyzing structural changes or plastic flow during deformation.

We simulate x-ray diffraction by assuming a monochromatic incident beam of x-rays is absorbed by each atom and instantaneously re-emitted as a spherical wave. The phase of the re-emitted wave is determined by the distance between the absorbing atom and the *x-ray source*. The re-emitted spherical wave then travels, with no further atomic interactions, to the target *plate camera*, interfering with other scattered waves to produce the familiar Laue diffraction pattern. The film plane is represented by an array of pixels, and the gray-scale brightness assigned to the pixel is proportional to the computed intensity. The resolution of the resulting patterns depends on three competing effects: the number of atoms in the sample,

'er

he
nd
he
to
its
a
1.
re
ic
d-

the thickness of the smallest region with a distinct phase, and the temperature of the sample. For the cold crystal shown in Figure 2 it is clear that 512 atoms provide sufficient resolution. In the results we describe in the next section we have combined the diffraction analysis with the calculation of the pair correlation function and plane-cutting views of the sample in real space to detect a phase transition within a region only a few atomic layers in size.

(a) N=64   (b) N=512   (c) N=1728
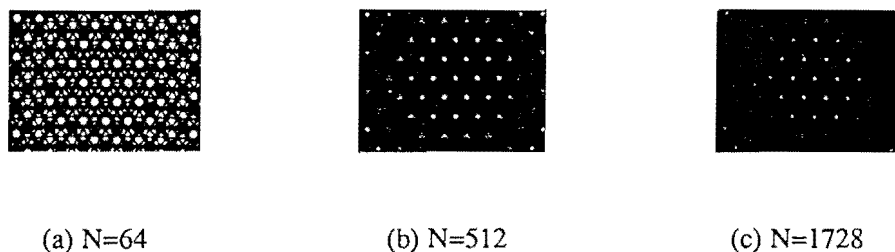
Figure 2. Size dependence of diamond-structure diffraction patterns, where N is the total number of atoms.

Computed difraction patterns from atomic co-ordinates generated from a Wooten-Weaire[5] model of amorphous silicon result in the diffuse ring structure shown in Figure 3. However, the diffuse ring patterns generated experimentally by an amorphous material or a collection of very small polycrystals are sometimes so similar as to be indistinguishable. The fundamental structural differences between these structures lead to characteristic pair correlation functions: the number of particles in a radial shell dr divided by r. This function has a series of sharp peaks (e.g., the first peak corresponds to the nearest neighbor distance). The third peak is a measure of crystallinity in the sample. A sharp third peak corresponds to the crystalline phase. and the disappearance of this peak corresponds to the amorphous phase. We use this characteristic of the pair correlation function along with the computed diffraction patterns in the results presented below to analyze the phase behavior of indented silicon.

n

ns
ie
ve
of
1.
ds

is
ie
ty
ie
ie
le
ie
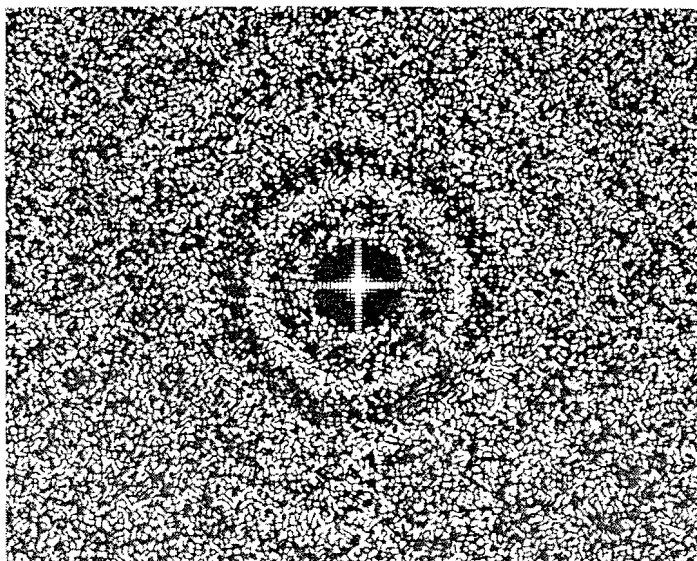
Figure 3. Computed diffraction pattern of simulated amorphous silicon, using the Wooten-Weaire model for the amorphous structure.

RESULTS

Experimental measurements[6,7] suggest a crystalline to amorphous phase transition. We present here the results for crystal indentations, at temperatures one half the melting temperature and near melting, with a smooth indentor model, and at an indentor speed corresponding to one thirtieth of the longitudinal sound speed. Figure 4 shows a comparison of diffraction from the undeformed and deformed crystal in the vicinity of the indentor.
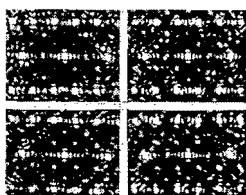
(a) These patterns represent the undeformed crystal below the indentor tip.
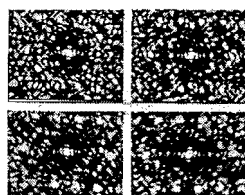
(b) The indentor tip is at the center of these four patterns.

Figure 4. Diffraction patterns at the end of crystalline indentation.

The patterns for the deformed crystal represent the center section of the crystal which includes the tip of the indentor. Each of the four patterns is calculated from a cubic volume containing roughly 175 atoms with the bottom surface of each volume lying on the midplane of the crystal. Diffraction patterns in adjacent volumes on the midplane match the patterns generated from undeformed crystal. Weak diffuse rings, similar to those calculated for the amorphous Wooten-Weaire model, are apparent in spite of the thermal fluctuations and the limited resolution. We have calculated the pair correlation function for both sets of diffraction patterns. The results are shown in Figure 5.
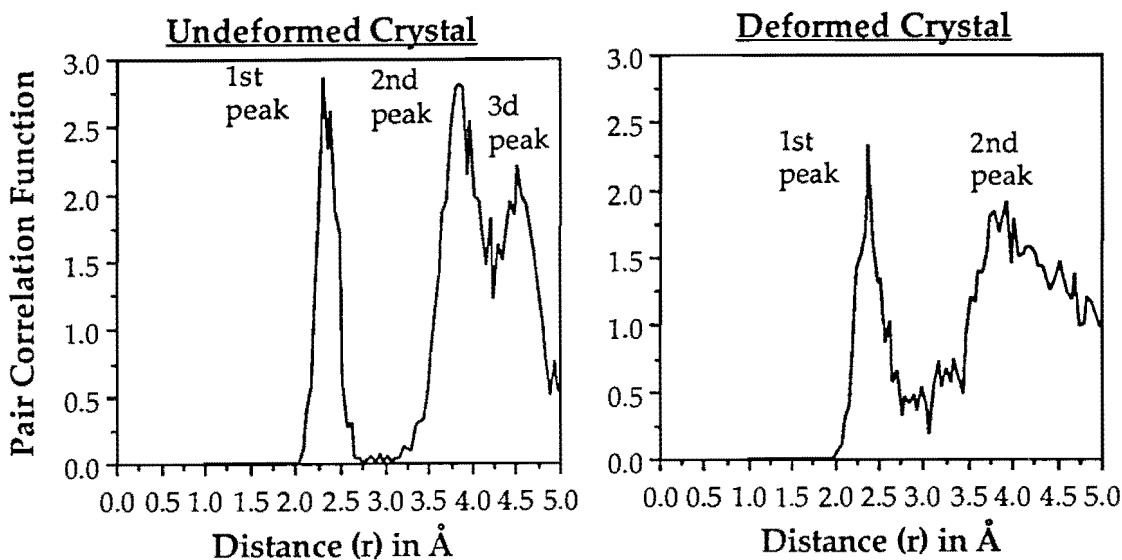
Figure 5. Pair correlation function in the volume in the upper left pattern of Figure 4a and 4b.

From the absence or weak presence of the third peak for the patterns near the indentor, we can conclude the region is partially amorphous. The same conclusion follows from an inspection of cut-away photographs. See Figure 6.
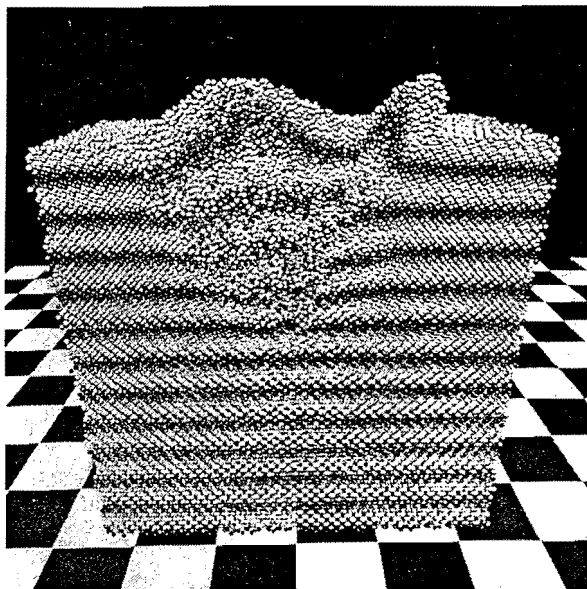
Figure 6. A cut-away view at the end of the indentation showing the plastic structure of the crystal in the region of the indentation.

Such real-space figures clearly show an amorphous plastically-worked zone in the vicinity of the indentor and in the characteristic surface bulges. Color, as a diagnostic, reveals that the bulges are buckled surface rather than upwelling bulk material.

The work of indentation is the sum of the elastic deformation energy, the surface energy, and the plastic energy. Both the surface and elastic energies are proportional to the square of the displacement and the displacement is proportional to the depth of the tetrahedral-indentor volume. The plastic energy density is roughly equal to the yield stress, Y, so that the plastic energy varies as the cube of the indentation depth, D. Data for eight runs are shown in Figure 7.

The curves are identified by four sets of initials:

A=Amorphous vs.
X=Crystalline.

R=Rough vs.
S=Smooth indentor model.

Indentor speeds:
F=Fast $1/30\ c_L$ vs.
S=Slow $1/300\ c_L$.

C=Cold $kT = 0.01$ vs.
W=Warm $kT = 0.03$ vs.
H= Hot $kT = 0.06$.
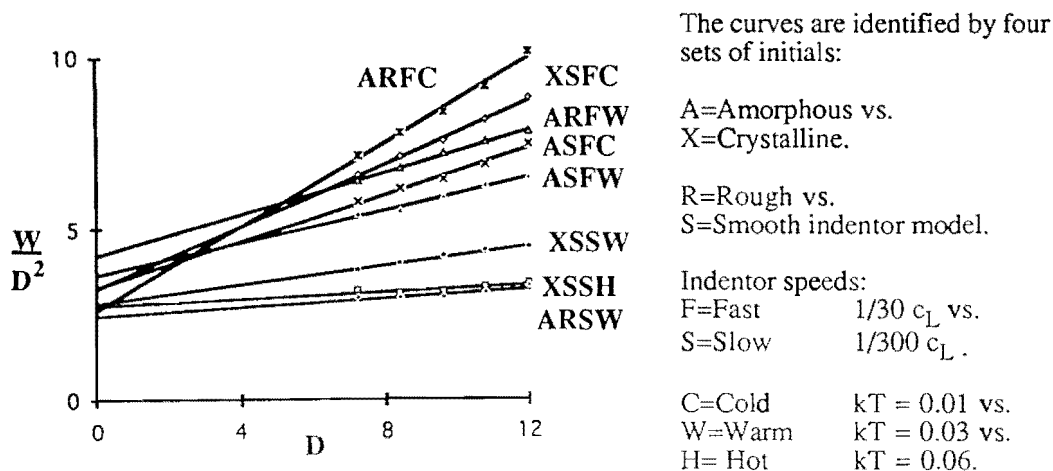
Figure 7. Variation of the reduced work of indentation, W_{total}/D^2 as a function of D. The intercept gives an estimate of the combined elastic and surface energies while the slope is the plastic yield strength. The energy and length scales are given in Stillinger-Weber units[4] (50kcal/mole and 0.21 nm).

From the analysis above, the work of indentation, W, satisfies the relationship,

$$W/D^2 = \alpha + YD .$$

The simulated data fit this relationship within 1% and provide estimates of the yield strength. The yield strengths range from 25 kilobars to 250 kilobars depending on structure, rate of deformation, and temperature.

So far all our specimens have been too small for massive crack formation. Because crack energy varies as $N^{2/3}$ while stored deformation energy varies as N, it is clear that somewhat larger-scale simulations will define the brittle-ductile transition for indentation. Hybrid models[3] which include atomistic and continuum regions are a powerful means for solving such mesoscopic-scale problems.

ACKNOWLEDGMENT

REFERENCES

1. W. G. Hoover, Computational Statistical Mechanics (Elsevier, Amsterdam, 1991), p. 255.
2. B. L. Holian, A. J. De Groot, W. G. Hoover, and C. G. Hoover, Phys. Rev. A, **41**, 4552 (1990).
3. W. G. Hoover, A. J. De Groot, and C. G. Hoover, Comp. in Phys., **6**, 155 (1992).
4. F. H. Stillinger and T. A. Weber, Phys. Rev. B, **31**, 5262, (1985).
5. F. Wooten and D. Weaire, Solid State Physics **40**, 1 (1987).
6. D. R. Clarke, M. C. Kroll, P. D. Kirchner, R. F. Cook, and B. J. Hockney, Phys. Rev. Letts. **60**, 2156 (1988).
7. K. Minowa and K. Sumino, Phys. Rev. Letts. **69**, 320 (1992).